

Everything everywhere all at once: A detailed study of GW230529

KOUSTAV CHANDRA ¹, ISH GUPTA ¹, ROSSELLA GAMBA ^{1,2}, RAHUL KASHYAP ¹, DEBATRI CHATTOPADHYAY ³,
ALEJANDRA GONZALEZ ⁴, SEBASTIANO BERNUZZI ⁴, AND B.S. SATHYAPRAKASH ^{1,5,3}

¹*Institute for Gravitation & the Cosmos and Physics Department, The Pennsylvania State University, University Park PA 16802, USA*

²*Department of Physics, University of California, Berkeley, CA 94720, USA*

³*School of Physics and Astronomy, Cardiff University, Cardiff, CF24 3AA, United Kingdom*

⁴*Theoretisch-Physikalisches Institut, Friedrich-Schiller-Universität Jena, 07743, Jena, Germany*

⁵*Department of Astronomy and Astrophysics, Penn State University, University Park PA 16802, USA*

ABSTRACT

This study investigates the origins of GW230529, delving into its formation from massive stars within isolated binary systems. Utilizing population synthesis models, we present compelling evidence that the neutron star component forms second. However, the event’s low signal-to-noise ratio introduces complexities in identifying the underlying physical mechanisms driving its formation. Augmenting our analysis with insights from numerical relativity, we estimate the final black hole mass and spin to be approximately $5.3 M_{\odot}$ and 0.53, respectively. Furthermore, we employ the obtained posterior samples to calculate the ejecta mass and kilonova light curves resulting from r-process nucleosynthesis. We find the ejecta mass to range within $0\text{--}0.06 M_{\odot}$, contingent on the neutron star equation of state. The peak brightness of the kilonovae light curves indicates that targeted follow-up observations with a Rubin-like observatory may have detected this emission.

1. INTRODUCTION

Electromagnetic observations have played a pivotal role in constraining the mass spectrum of neutron stars (NSs) and black holes (BHs). Notably, X-ray and radio observations have consistently indicated that the maximum mass of NSs falls within the range of $2\text{--}2.6 M_{\odot}$, while BH masses have been found to exceed $5 M_{\odot}$ (Antoniadis et al. 2016; Alsing et al. 2018; Farr & Chatzioanou 2020; Fonseca et al. 2021; Romani et al. 2022; Bailyn et al. 1998; Ozel et al. 2010; Farr et al. 2011). Consequently, these detections have implied a notable absence of compact binaries within the mass range of $2.6\text{--}5 M_{\odot}$, a notion reinforced by initial gravitational-wave (GW) observations Abbott et al. (2019a, 2021). However, Supernova (SNe) simulations have predicted the existence of BHs within this gap (Fryer et al. 2012). Furthermore, the recent observation of the binary merger GW230529_181500 (hereafter referred to as GW230529) has provided conclusive evidence for the existence of compact objects within this mass range (LVK 2024).

This event was observed only in LIGO Livingston (Aasi et al. 2015), with a signal-to-noise ratio (SNR) $\gtrsim 11$ and a low false alarm rate (FAR) of less than one

event per thousand years. Assuming GW230529 is the result of the merger of a black hole–neutron star binary on a quasi-circular orbit, the data are consistent with the merger of two compact objects with masses $3.6_{-1.2}^{+0.8} M_{\odot}$ and $1.4_{-0.2}^{+0.6} M_{\odot}$ (90% credible intervals), making it the most symmetric mixed compact binary merger detected via GWs.

Measuring these mass parameters is part of the inverse problem. Other parameters of astrophysical interest include, but are not limited to, the components’ spins, the tidal properties and the remnant properties. A Bayesian inference approach is typically employed, which necessitates model evaluations to reliably infer the posterior distribution for the parameters that characterize the observed signal. While the data containing GW230529 was matched against several state-of-art GW signal models, LVK (2024)’s initial analysis assumed priors that are effectively flat in component masses and spin magnitudes. These astrophysically-agnostic priors do not provide information about GW230529’s possible formation mechanism.

Therefore, LVK (2024) reweighed the posterior samples using a few astrophysically-informed mass and spin distributions to constrain the source properties (Fishbach et al. 2020; Farah et al. 2022; Ray et al. 2023). They unequivocally observed that the compo-

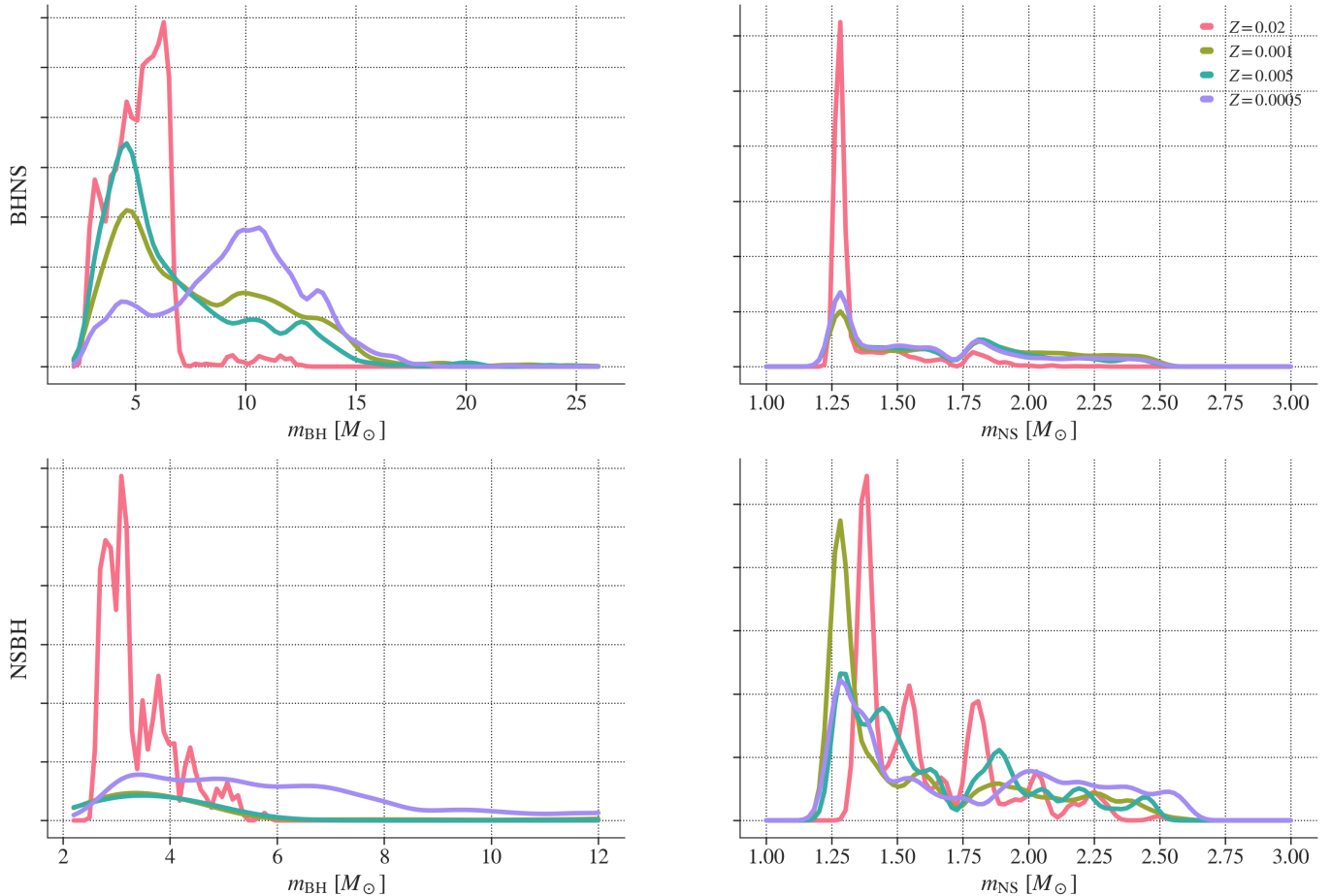


Figure 1. Predicted component mass distributions for BHNS (top panel) and NSBH systems (bottom panel) across varying sub-solar metallicities, as outlined in [Chattopadhyay et al. \(2021\)](#). As can be observed, NSBH systems tend to produce binaries with lighter BHs across different metallicity.

nent masses inferred for GW230529 differ across different population-informed priors, demonstrating that the choice of prior significantly impacts the inferred masses and spins of the GW230529’s source. This is expected, given the event’s low SNR. Therefore, it is necessary to determine whether the data support a given model, as strong priors might drive the posteriors to arbitrary values at the expense of Bayesian evidence.

Also, the employed astrophysically-informed priors are phenomenological and contain only an *observationally constrained* understanding of stellar and binary evolution. Further, [Zhu et al. \(2024\)](#) found that the GW230529’s masses are close to those predicted in their BHNS population simulations.

In this article, we re-analyze the data containing GW230529 with population-informed priors to provide conclusive insights into the probable physical processes underlying this binary formation. Leading formation models of GW230529-like systems include the isolated evolution of massive binary stars in galactic fields via the Common Envelope (CE) and the dynamical as-

sembly aided by either a tertiary companion, multiple exchanges in dense clusters or gas-assisted migration (see [Mandel & Broekgaarden \(2022\)](#) and references therein). While direct collapse leading to the formation of the primary component is unlikely due to its low mass, recent population synthesis models have argued the plausibility of such systems arising from isolated evolution scenarios ([Chattopadhyay et al. 2021](#); [Broekgaarden et al. 2021](#); [Broekgaarden & Berger 2021](#); [Chattopadhyay et al. 2022](#)). However, these models have major uncertainties such as mass loss, mass transfer and the impact of supernova explosions, resulting in a broad spectrum of merger rate predictions and varying mass and spin distributions.

We describe our methodology in [Sec. 2](#), utilizing it subsequently in [Sec. 3.1](#) to ascertain the nature of the merger—specifically, whether the NS or BH formed first. Consequently, in [Sec. 3.2](#), we employ the evidence ratio of posterior samples and the distribution of log-likelihood ratios to distinguish between various forma-

tion models, shedding light on the most likely formation mechanism of GW230529.

We then use the posterior samples corresponding to these models to analyse the characteristics of the remnant BH, as detailed in Sec. 4.1. Our analysis is conducted using a selection of Equation of States (EoSs) that adhere to current astrophysical and nuclear constraints (Breschi et al. 2024). Furthermore, this section assesses the probability of NS’s tidal disruption during the merger.

Subsequently, in Sec. 4.2, we present the range of ejecta masses that inform the r-process synthesis resulting from such events. Our analysis incorporates four fiducial EoSs, namely APR4 (Akmal et al. 1998), SLy (Chabanat et al. 1998; Douchin & Haensel 2001), DD2 (Typel et al. 2010; Hempel & Schaffner-Bielich 2010) and H4 (Glendenning & Moszkowski 1991; Lackey et al. 2006; Read et al. 2009).

Finally, in Sec. 4.3, we compute the lightcurves associated with kilonovae (KNe) for the event under consideration. While these lightcurves may be fainter compared to those observed in the GW170817 event, they may be detectable through targeted searches using observatories such as Rubin Observatory (Ivezić et al. 2019). Lastly, in Sec. 5, we conclude our findings.

2. METHODS

We infer GW230529’s properties by analysing 128s of LIGO Livingston data using the Bayesian parameter estimation (PE) library BILBY (Ashton et al. 2019) and the posterior sampling algorithm DYNESTY (Speagle 2020). We assume a noise power spectrum given by the median estimate provided by BAYESLINE (Littenberg & Cornish 2015) and use frequencies in the range of 20 – 1792 Hz for evaluating the GW Transient log-likelihood ratio $\ln \mathcal{L}$. Furthermore, to speed up the likelihood evaluation, we include heterodyning (also known as relative binning; (Cornish 2010; Zackay et al. 2018; Cornish 2021; Krishna et al. 2023)). For our analysis, we use the quasi-circular frequency-domain phenomenological waveform model, IMRPhenomNSBH (Foucart et al. 2013, 2014; Khan et al. 2016; Dietrich et al. 2019; Thompson et al. 2020). This waveform approximates signals using the dominant (quadrupole) harmonic and is specifically designed to model GWs emanating from black hole–neutron star binary mergers with mass ratios ranging from equal-mass up to $q = m_{\text{BH}}/m_{\text{NS}} = 15$. It also incorporates BH spins up to a dimensionless value of $\chi_{\text{BH}} = 0.5$ and includes matter-effects through tidal parameters Λ_{NS} ranging from 0 to 5000. We assess the impact of waveform systematics in

App. A, finding them to be negligible for the purposes of our study.

However, unlike the original analyses, we exclude the marginalization over the systematic error in the measured astrophysical strain due to the detector calibration. This error is sub-dominant to the systematic errors from waveform modelling and prior choices, and we, therefore, neglect it (Ashton & Dietrich 2022). Furthermore, as discussed in Sec. 3.2, we apply astrophysically motivated mass and spin priors while using uninformative priors for all other parameters. It is important to note that, for all our analysis, we utilise the BH and NS masses viz m_{BH} and m_{NS} priors derived from population synthesis models as two distinct, one-dimensional independent priors.

While various assumptions may be made to model the formation pathway of this system, one needs to determine the relative probability of two models (in this case, binary formation process) given the data. The Bayesian evidence, \mathcal{Z} , quantifies this support. Varying prior assumptions can yield differing parameter estimates; therefore, the Bayes Factor, $\text{BF}_B^A = \mathcal{Z}_A/\mathcal{Z}_B$, indicates whether the prior assumption A is favoured or disfavoured compared to B based on the data. This comparison is particularly crucial as strong prior assumptions may bias the posteriors towards potentially arbitrary values at the expense of the evidence. Furthermore, we also compare the log-likelihood ratio distribution since certain models allow for broader priors and incur a higher Ockham penalty.

3. ASTROPHYSICAL IMPLICATIONS

LVK (2024) found no conclusive evidence either supporting or refuting the presence of tidal effects in the GW230529 signal. This makes it difficult to determine the nature of the compact objects involved. However, they showed that the (lighter) secondary component appears to be a NS, while the (heavier) primary is likely a BH, when using observationally constrained priors. In this section, we investigate which of the binary components formed first and determine their formation mechanism.

3.1. BHNS or NSBH?

Black hole–neutron star binaries can generally be divided into two categories: (1) BHNS mergers, where the BH forms first, and (2) NSBH mergers, in which the NS forms first. While BHNSs are the dominant binaries according to population synthesis studies (Chattopadhyay et al. 2021), NSBHs are more exciting as they can form radio pulsars, generate KN (Barbieri et al. 2020), and lead to precise measurement of NS spins (Gupta 2024).

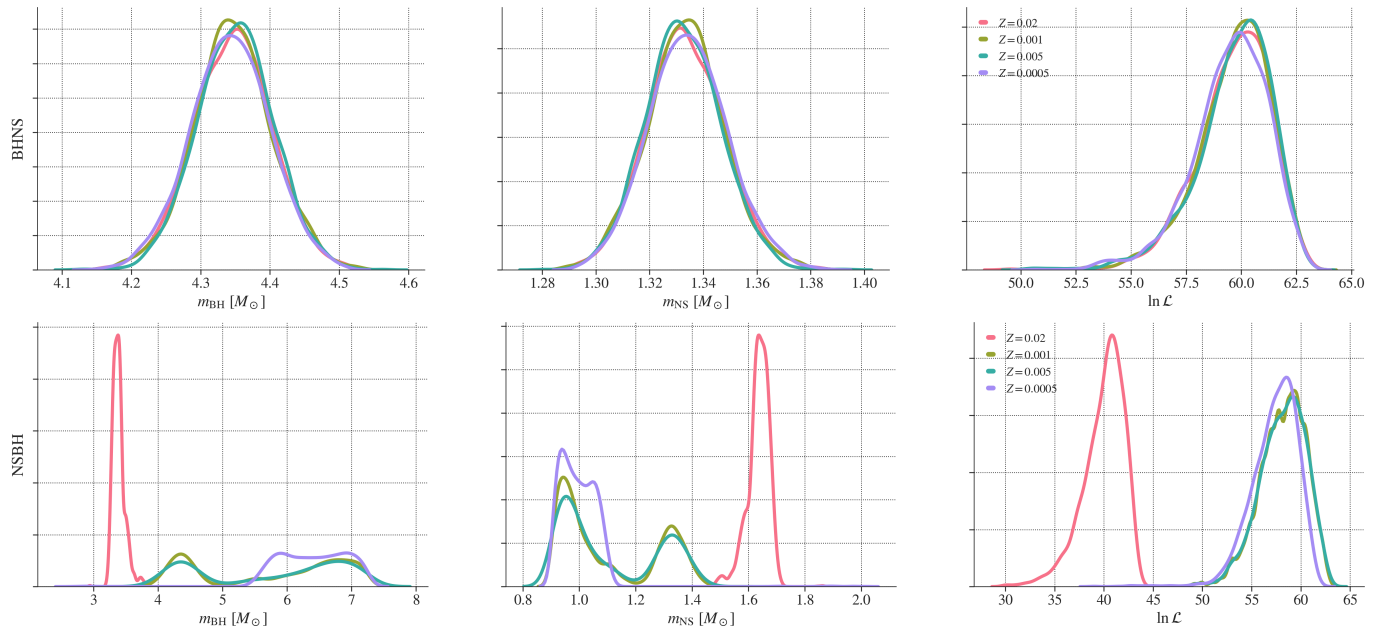


Figure 2. Posterior densities for the mass of GW230529 as inferred using population-inspired BHNS (top panel) and NSBH (bottom panel) priors described in Sec. 3.1. In the right-hand column, we include the log-likelihood ratio distribution.

To discriminate between the two, we analyze GW230529 using different predicted distributions of the detectable BHNS and NSBH masses and spins for different metallicity choices ($Z = 0.02, 0.001, 0.005, 0.0005$) from the base model of Chattopadhyay et al. (2022). These models are expected to be representative of the population of such binaries obtained from GW observations.

As can be seen in Fig 1, the BHNS (top panel) and NSBH (bottom panel) systems exhibit distinct mass spectra, with BHs in BHNS systems being more massive. This is because the heavier star evolves faster and remains massive enough to form a BH even after the mass transfer (Hurley et al. 2000; Belczynski et al. 2010). In contrast, NSBH systems have more mass-symmetric progenitors, more so at higher metallicities. The heavier star transfers enough mass to its companion to form a NS, whereas its companion becomes a BH. However, at lower metallicities, reduced stellar winds lead to reduced mass loss, creating larger BHs that merge in a shorter time scale (Hurley et al. 2000).

We use BH spins derived from fits in Chattopadhyay et al. (2021) for NSBH mergers but restricted to $\chi_{\text{BH}} = 0.5$ as IMRPhenomNSBH is not calibrated for $\chi_{\text{BH}} > 0.5$. Moreover, attaining spins greater than this would require an unphysical amount of matter accretion (Mandel & Fragos 2020). Although tidal synchronization can lead to higher BH spins, the fraction of such binaries is small (Chattopadhyay et al. 2021). For the BHNS case, we set $\chi_{\text{BH}} = \chi_{\text{NS}} = 0$ as the rotational velocities of neutron star are anticipated to diminish over

time due to electromagnetic radiation (Fragos & McClintock 2015; Ma & Fuller 2019). As ground-based GW observatories are only expected to detect these binaries close to the merger, we assume that the BH and NS objects have negligible spin. Thus, for the second analysis, we effectively assume that the *source of GW230529 is a non-spinning BHNS binary*.

Figure 2 shows an obvious trend; the log-likelihood ratio distribution associated with the BHNS (top panel) has a higher median log-likelihood ratio value and contains a prominent peak compared to the NSBH case (bottom panel) for the same metallicity choices. Further, the BHNS hypothesis is preferred with a $\ln \text{BF}_{\text{NSBH}}^{\text{BHNS}} > 17(9)$ for metallicity choice of $Z = 0.02(0.0005)$. Therefore, we will assume that GW230529 is a BHNS merger for the remainder of the article. Note that our results are robust against waveform systematics (See App. A).

3.2. Constraints on binary evolution

The pathway leading to BHNS mergers is still debated. The prevailing hypothesis suggests that these mergers arise from two massive stars that were born in a binary and evolved in isolation, typically involving the CE episode that tightens the binary’s orbit (Mandel & Broekgaarden 2022). However, accurately estimating the rates of these mergers is challenging for several reasons.

Firstly, the physical processes that govern the evolution of massive binary star systems, including the dynamics of the CE phase (Ivanova et al. 2013), mass

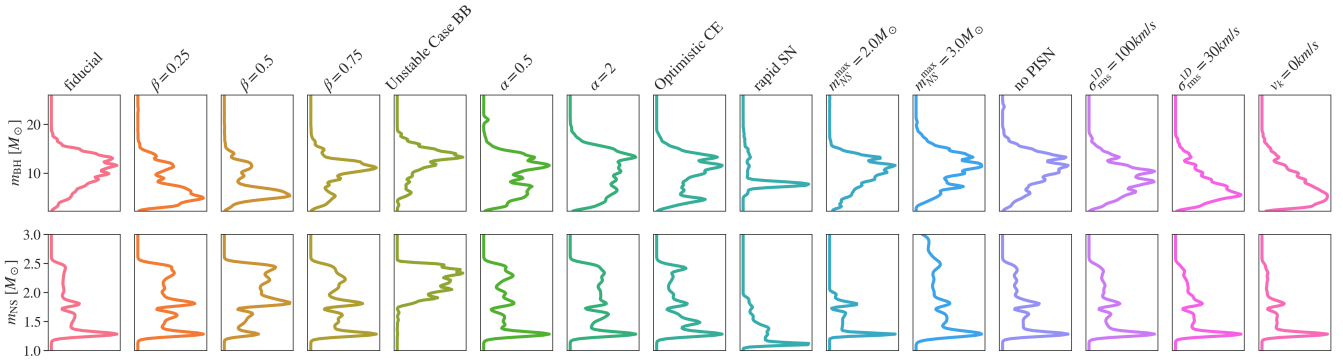


Figure 3. Predicted BHNS component mass distributions. Each row shows the 15 different population synthesis variations used by Broekgaarden et al. (2021).

transfer efficiency between binary components, and the kicks imparted to stars during Supernova (SNe), are complex and poorly understood, leading to considerable uncertainty (Belczynski et al. 2022). Secondly, uncertainties arise due to the star formation rate and the metallicity distribution within star-forming gas across cosmic time (Langeroodi et al. 2023; Garcia et al. 2024). Together, they significantly impact the detectable BHNS mass distributions.

Since we are interested in determining the physical process leading to GW23059’s formation, we only focus on the uncertainties related to the physical processes. To that end, we, following Broekgaarden et al. (2021), assumed 15 different binary population synthesis predictions for BHNS mass distribution. These models implement variations to the *fiducial* model in different aspects of physics relevant to the binary evolution, such as mass transfer efficiency between binary components and the kicks imparted to the stars. We briefly summarise them below.

The $\beta = 0.25, 0.5, 0.75$ models assume fixed mass transfer efficiencies. These models represent the fraction of mass lost by the donor star that its companion accretes. On the other hand, the “unstable case BB” model involves an unstable mass transfer phase from a stripped post-helium-burning star onto a BH.

For the $\alpha = 0.5$ and $\alpha = 2$ models, a pessimistic CE scenario is assumed, where the donor stars struggle to successfully eject their envelopes, resulting in efficiency parameters of 0.5 and 2, respectively. Conversely, the “optimistic” CE scenario posits that these systems can survive such challenges.

To avoid creating a remnant mass gap between NSs and BHs, which contradict observations from X-ray binaries, Broekgaarden et al. (2021) use a delayed remnant mass prescription in their simulations. However, the “rapid SNe” model adopts a faster remnant mass prescription and is consistent with current observations.

The models labeled as $m_{\text{NS}}^{\text{max}} = 2M_{\odot}$ and $m_{\text{NS}}^{\text{max}} = 3M_{\odot}$ set the maximum mass of NS to 2 and $3M_{\odot}$, respectively. It’s worth noting that the latter case may be considered unrealistic since the maximum mass supported by current EoS for non-rotating NS is $\lesssim 2.9M_{\odot}$ (Godzieba et al. 2021).

The “no PISN” prescription excludes the pair-instability process, responsible for the scarcity of first-generation BHs with masses between $65\text{--}120M_{\odot}$. Additionally, the $\sigma_{\text{cc}} = 30 \text{ km/s}$ and $\sigma_{\text{cc}} = 100 \text{ km/s}$ prescriptions explore variations of natal kicks compared to the one-dimensional root-mean-square velocity dispersion of $\sigma_{\text{cc}} = 265 \text{ km/s}$ used in the fiducial model. These lower values can occur in ultra-stripped SNe and electron-capture SNe, leading to reduced binary disruption. Finally, the $v_{\text{k,BH}} = 0 \text{ km/s}$ assumption posits that BHs receive no supernova natal kicks.

Fig 4 summarises our findings when assuming these populations. We observe that, except for the “unstable case BB” and “rapid SNe” models, the inferred posteriors are largely in agreement with each other. This alignment was anticipated, given that these two population models restrict the BH mass to a range outside the support for this signal. Moreover, we do not observe any trends in the log-prior distribution for the other models, which indicates that all the information about the evidence for and against binary evolution is contained in the distribution of the log-likelihood ratio. But we also do not observe any differences in the shape and location of the log-likelihood ratio distribution, indicating that all models are equally likely. This is not surprising since the signal’s SNR is low. Finally, it is noteworthy that, for the majority of our analysis, we determine the BH and NS masses to be $m_{\text{BH}} = 4.3^{+0.08}_{-0.09}M_{\odot}$ and $m_{\text{NS}} = 1.4^{+0.02}_{-0.02}M_{\odot}$, respectively, while finding that the $\ln \text{BF}_{\text{pop-agnostic}}^{\text{fiducial}} \sim 1$.

4. MULTIMESSENGER PREDICTIONS

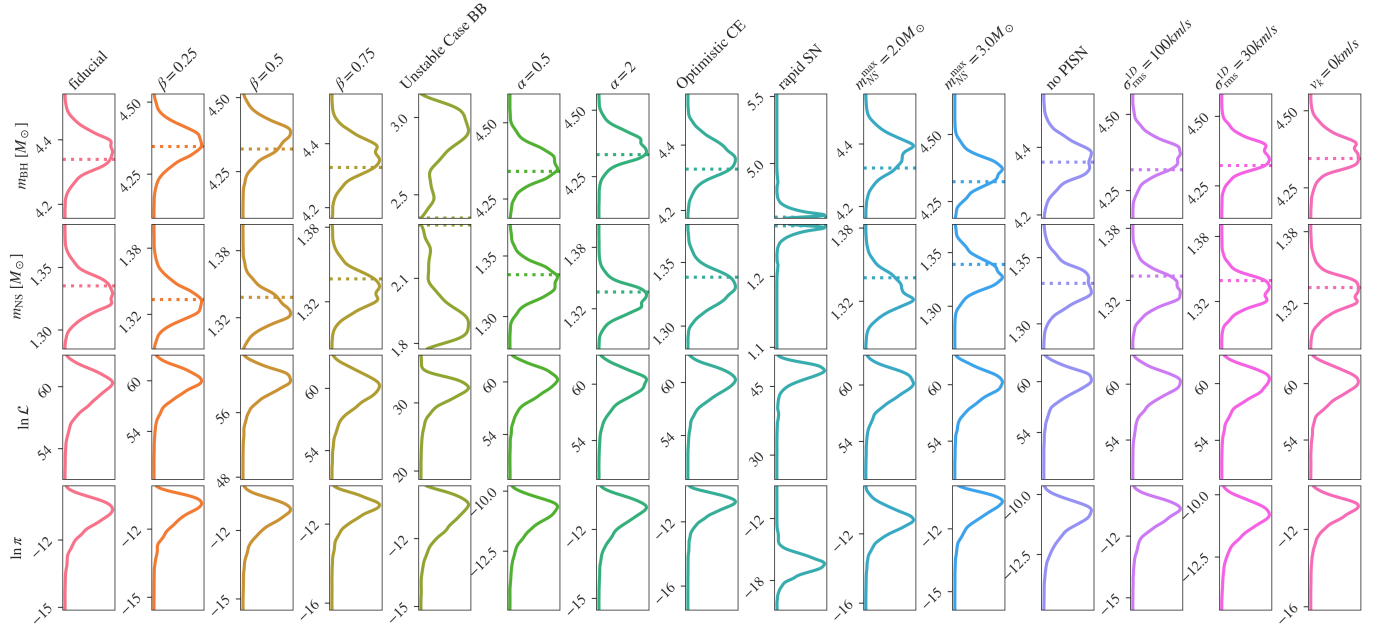


Figure 4. Posterior densities for the mass of GW230529 under different binary evolution assumptions. We also include the distributions of the log-likelihood and log-prior of the posterior samples. The dotted lines in the first two rows denote the maximum likelihood estimates of m_{BH} and m_{NS} respectively.

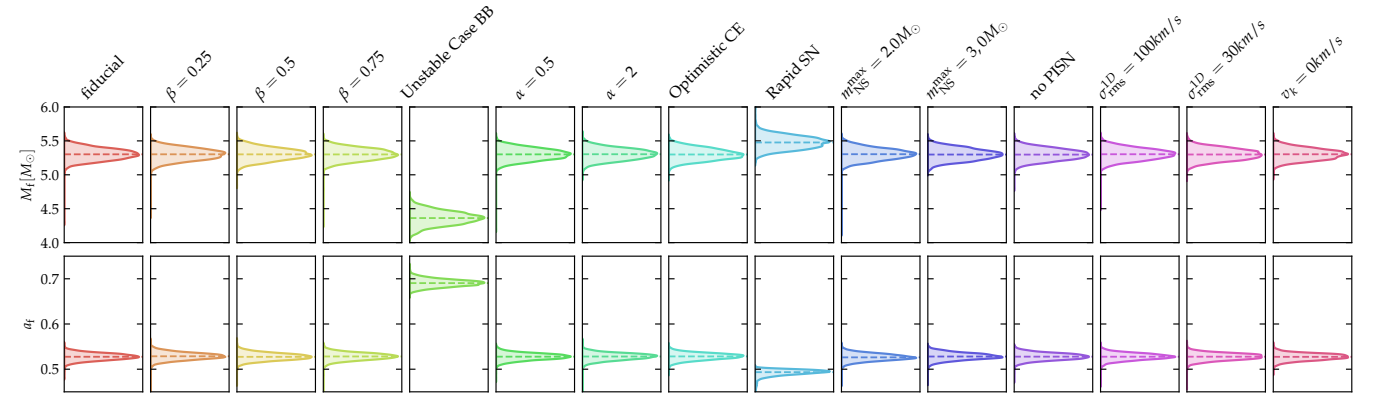


Figure 5. Posterior densities for the remnant BH mass and spin under different binary evolution assumptions. These quantities are computed from NR fits of BHNS binaries, using the posteriors from Sec. 3.2 and the EoS information coming from multi-messenger analyses of GW170817 and AT2017gfo. For most of the scenarios considered we find $M_f = 5.3^{+0.1}_{-0.1} M_\odot$ and $a_f = 0.53^{+0.01}_{-0.01}$.

4.1. Remnant properties

Assuming GW230529 is a BHNS merger, estimates of the final mass and spin of the remnant BH can be made using the models of Zappa et al. (2019); Gonzalez et al. (2023). Rather than employing the uninformative posteriors on the tidal parameters obtained from our PE, we combine samples obtained using the the IMRPhenomNSBH waveform with the EoSs of Breschi et al. (2024). This set was obtained by performing joint analysis of GW170817 (Abbott et al. 2017, 2019b) and AT2017gfo (Villar et al. 2017), including information

from NR in the KNe model employed and folding in pulsar mass and radii measurements (Miller et al. 2021; Romani et al. 2022; Vinciguerra et al. 2024).

Figure 5 shows the predicted remnant property distribution for various formation model assumptions. We find that all models, with the exception of the “Unstable case BB” and “the Rapid SNe”, predict the formation of a $M_f = 5.3^{+0.1}_{-0.1} M_\odot$ BH remnant, with a dimensionless spin $a_f = 0.53^{+0.01}_{-0.01}$.

Applying the classification proposed in Sec. II of Gonzalez et al. (2023), we further find high probability

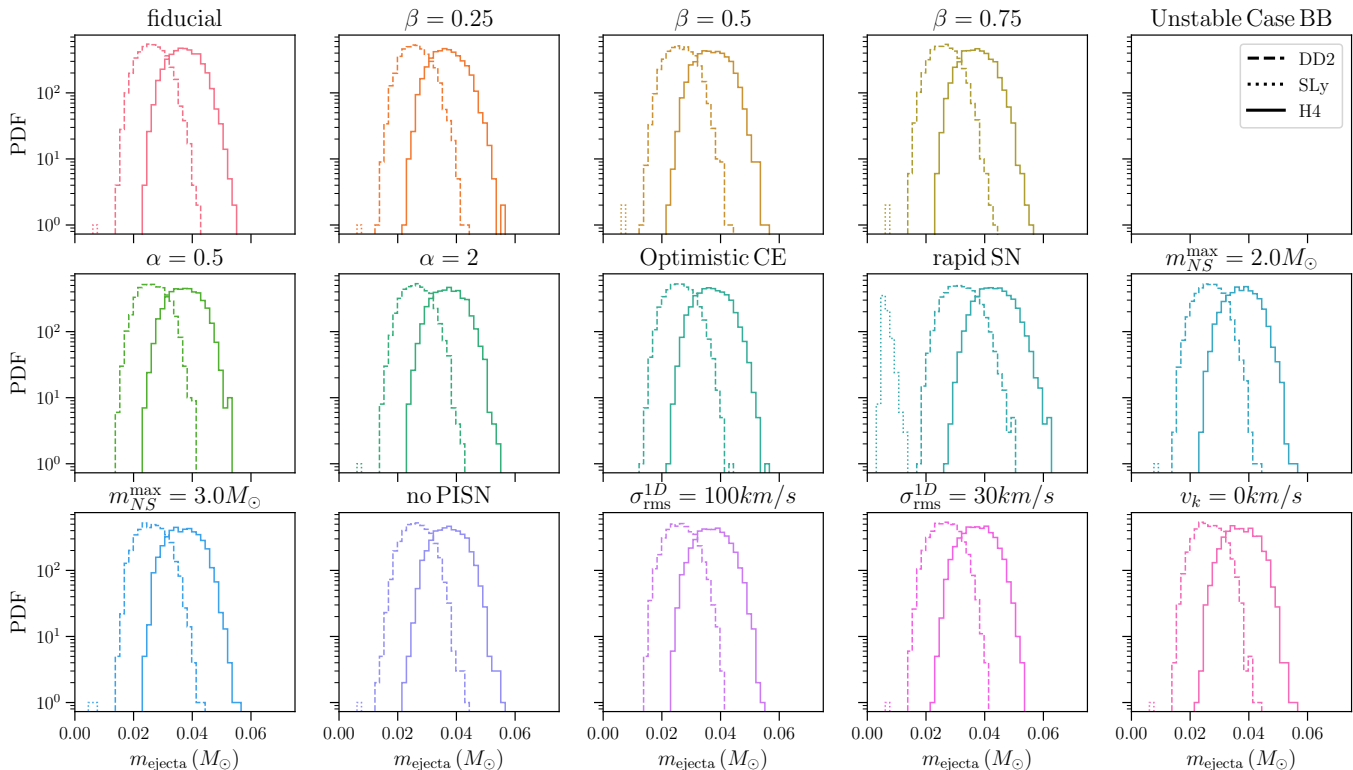


Figure 6. The probability distribution function (PDF) for the total ejecta mass for different EoS and corresponding to the various population models. No ejecta was obtained for the APR4 EoS.

($\geq 99\%$) of the NS being at least partially tidally disrupted during the coalescence, with about 13% probability of such disruption happening far from the system’s innermost circular orbit. This value is consistent with the findings of LVK (2024), indicating that one would expect to observe a suppressed but nonetheless present ringdown signal and a possible electromagnetic counterpart.

4.2. Ejecta Mass

During a BHNS merger, the NS can get tidally disrupted. The neutron-rich ejecta from such disruption can emit KNe (Metzger 2017) provided the NS disrupts before it enters the innermost circular orbit (R_{ISCO}) corresponding to the BH. If the NS sheds mass after crossing this orbit, the BH swallows the ejecta, producing no KN. Hence, the distance at which the NS starts shedding mass must be greater than R_{ISCO} to produce a transient. The ratio of the mass-shedding radius and R_{ISCO} increases with the BH spin and decreases with the binary’s mass ratio and the NS’s compactness for aligned spin. For anti-aligned cases, the mass-shedding limit increases significantly, disfavoring tidal disruption. Thus, mass-symmetric binaries with a rapidly spinning BH are conducive to generating KNe. Similarly, less compact NSs (coming from stiff EoS) are easier to disrupt for

aligned spin case, which is also favorable for KNe production. We utilize the isotropic framework proposed in (Arnett 1980, 1982; Chatzopoulos et al. 2012; Villar et al. 2017; Kashyap et al. 2019; Gupta et al. 2024) to calculate KN light curves resulting from r-process nucleosynthesis in BHNS mergers (see Kawaguchi et al. 2024 for comparison and angle-dependence on light curve). The KNe lightcurves are characterized by the ejecta mass, velocity and opacity, which are informed by and related to the binary parameters using up-to-date NR simulations (Kyutoku et al. 2018; Barbieri et al. 2019; Lattimer & Schramm 1976, 1974; Kyutoku et al. 2021; Krüger & Foucart 2020). We use the posterior samples obtained in the Sec. 3.2 and calculate the mass of total ejecta, dynamical ejecta, and unbound disk ejecta using the fits from Krüger & Foucart (2020) and Raaijmakers et al. (2021).

This calculation is performed using four different EoSs: APR4 (Akmal et al. 1998), SLy (Chabanan et al. 1998; Douchin & Haensel 2001), DD2 (Typel et al. 2010; Hempel & Schaffner-Bielich 2010) and H4 (Glendenning & Moszkowski 1991; Lackey et al. 2006; Read et al. 2009) (see Fig. 10 in Appendix B for corresponding mass-radius curves). Among these, APR4 and SLy give relatively more compact NSs, whereas DD2 and H4 result in less compact ones. Thus, the latter two will produce

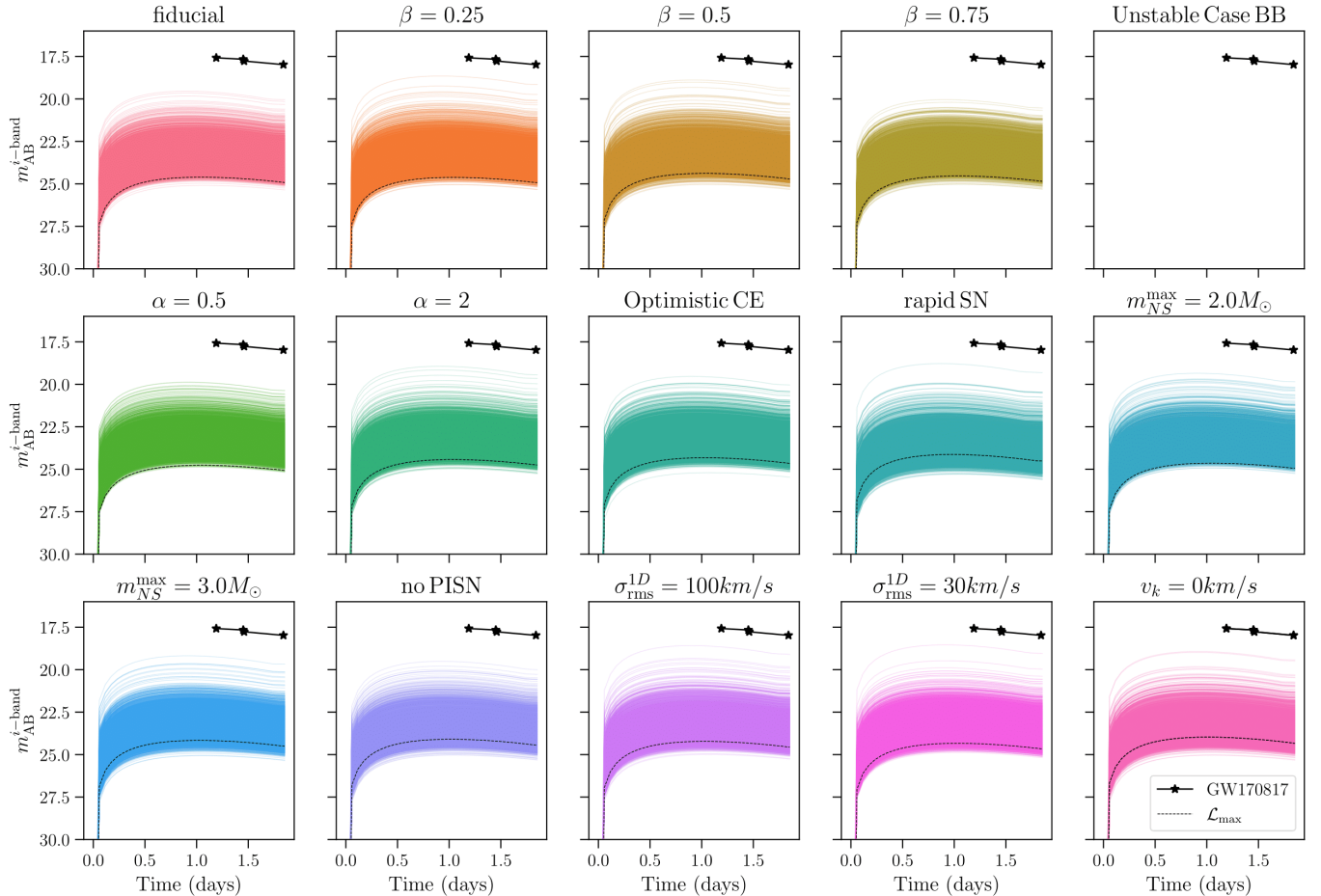


Figure 7. KNe light curves in the i -band corresponding to the different population models for the H4 EoS. The dotted line shows the light curve associated with the maximum likelihood parameter estimates for each model.

more ejecta than the former. We find that APR4 does not give any ejecta for samples corresponding to any population models. Fig. 6 shows the probability distribution of total ejecta for the remaining three EoS. Across population models, the total ejecta mass corresponding to SLy $\lesssim 0.01M_{\odot}$, DD2 $\lesssim 0.05M_{\odot}$, and H4 $\lesssim 0.07M_{\odot}$. Most ejecta are produced for the samples corresponding to the “rapid SNe” population model, which is due to its preference for a more symmetric binary (c.f. Fig. 4). On the other hand, the “Unstable Case BB” population model results in no ejecta, due to its preference for more massive (hence, more compact) NS. Note that both “rapid SNe” and “Unstable Case BB” population models are disfavored compared to others, as discussed in Sec. 3.2.

4.3. Kilonova Lightcurves

Choosing the most optimistic scenarios, namely those corresponding to H4 EoS, we calculate the bolometric KNe light curves (see Appendix B for DD2). We convert them to bandwise light curves for the *ugrizy* filters (see Gupta et al. (2023) and Appendix B for more details).

Figure 7 shows i -band curves together with the curve for maximum likelihood (\mathcal{L}_{\max}) binary parameters. We also compare the points from the detected light curve of GW170817 (Guillochon et al. 2017; Villar et al. 2017) in the i -band.

From Fig. 7, we note that only the “Unstable case BB” mass transfer population model does not support a KN after the merger, a population model disfavored by our analysis. For all other population models, the KN is expected to be considerably dimmer than the one observed for GW170817. This is expected, given that the KN flux is inversely proportional to the distance squared and that GW230529 is located approximately five times further than GW170817 (LVK 2024). For all population models, the curves corresponding to the \mathcal{L}_{\max} binary parameters prefer comparatively dimmer KNe, which is because the \mathcal{L}_{\max} parameters correspond to more mass-asymmetric binary located further away.

Focusing on the KNe properties, we note that the luminosity in the i -band peaks a day after the merger for all population models except “unstable case BB”. The

Table 1. The (optical) bandwise peak luminosities and decay in luminosity one day after peak for the KNe with \mathcal{L}_{\max} binary parameters corresponding to the “fiducial” population model and the H4 EoS. For comparison, the single-exposure (30 s) bandwise limiting magnitudes corresponding to the Rubin Observatory ($m_{\text{RO}}^{\text{lim}}$) are also listed.

| Band | $m_{\text{RO}}^{\text{lim}} (m_{\text{AB}})$ | Peak ($m_{\text{AB}})$ | Decay ($m_{\text{AB}})$ |
|----------|--|-------------------------|--------------------------|
| <i>u</i> | 23.9 | 26.63 | 1.85 |
| <i>g</i> | 25.0 | 25.80 | 1.04 |
| <i>r</i> | 24.7 | 25.05 | 0.59 |
| <i>i</i> | 24.0 | 24.61 | 0.35 |
| <i>z</i> | 23.3 | 24.27 | 0.16 |
| <i>y</i> | 22.1 | 24.04 | 0.10 |

peak luminosities corresponding to the \mathcal{L}_{\max} binary parameters lie in the range [23.97, 24.67] mag. For the “fiducial” population model and \mathcal{L}_{\max} binary parameters, Table 1 shows the bandwise peak luminosities and its decay. The latter is the absolute difference between the peak luminosity and one day after it.

To gauge the KNe detectability, we compare the peak luminosity in each band with the corresponding limiting magnitude ($m_{\text{RO}}^{\text{lim}}$) of the Rubin Observatory for a single, 30s long exposure. While the KNe in the *y*-band is the brightest, Rubin wouldn’t have observed it owing to its relatively poor sensitivity in this band. For the “fiducial” population model, peak luminosities in the *gri* bands come closest to the limiting magnitude threshold. However, a targeted observation with 600s exposure increases the limiting magnitude for the *g* and *i* bands to 26.62 and 25.62 (Gupta 2023; Branchesi et al. 2023), respectively, making the KNe visible in these bands.

5. CONCLUSIONS

In this work, we have studied the origins of GW230529, assuming that it is a binary formed via the classical isolated binary evolution via the CE phase. As discussed in Sec 3.2, by leveraging the BHNS binary population synthesis model from Broekgaarden et al. (2021), we present compelling evidence that the system’s properties are consistent with the predictions derived from the isolated binary evolution pathway of BHNS systems. However, due to the event’s relatively low SNR, we face difficulties in identifying the underlying physical mechanism driving its formation unequivocally. However, we could rule out with confidence certain formation mechanisms such as the one involving the “rapid SNe” or the “unstable case BB”.

Using our posterior samples and numerical fits from Zappa et al. (2019); Gonzalez et al. (2023), we infer the remnant’s mass and spin, finding that it is consistent

with a BH with $M_f \sim 5.3M_{\odot}$ and $\chi_f \sim 0.53$. We also predict that there is a $\gtrsim 99\%$ probability that NS is tidally disrupted during the merger and about 13% probability that such disruption occurs outside R_{ISCO} , leading to potential electromagnetic counterparts and a suppressed ringdown signal.

We compute KNe light curves using our population-informed posterior samples and the isotropic framework proposed by Arnett (1980, 1982); Chatzopoulos et al. (2012); Villar et al. (2017). We find that the *i*-band luminosity is dim enough not to be observed in a regular Rubin search but may be bright enough to be observed in a targeted one.

Overall, GW230529 is a notable addition to the growing population of compact binaries observed in the gravitational-wave window. It marks the first of many more events with components with masses between $\sim 3\text{--}5M_{\odot}$, the so-called “lower mass-gap” that divides the NS and BH population.

ACKNOWLEDGEMENTS

We thank Simon Stevenson and Aditya Vijaykumar for their comments and valuable suggestions. KC, IG, RK and BSS acknowledge the support through NSF grant numbers PHY-2207638, AST-2307147, PHY-2308886, and PHY-2309064. RG acknowledges support from NSF Grant PHY-2020275 (Network for Neutrinos, Nuclear Astrophysics, and Symmetries (N3AS)). DC is supported by the STFC grant ST/V005618/1. SB knowledge funding from the EU Horizon under ERC Consolidator Grant, no. InspiReM-101043372. DC and BSS thank the Aspen Center for Physics (ACP) summer workshop 2022 for setting up discussions that also contributed to this collaborative work. TEOBResumS is publicly available at https://bitbucket.org/eob_ihes/teobresums. The version employed in this work is tagged via the arXiv submission number of the paper itself. This research has made use of data, software and/or web tools obtained from the Gravitational Wave Open Science Center (<https://www.gw-openscience.org>), a service of LIGO Laboratory, the LIGO Scientific Collaboration, the Virgo Collaboration, and KAGRA. This material is based upon work supported by NSF’s LIGO Laboratory, which is a major facility fully funded by the National Science Foundation. LIGO Laboratory and Advanced LIGO are funded by the United States National Science Foundation (NSF) as well as the Science and Technology Facilities Council (STFC) of the United Kingdom, the Max-Planck-Society (MPS), and the State of Niedersachsen/Germany for support of the construction of Advanced LIGO and construction and operation of the GEO600 detector. Additional support

for Advanced LIGO was provided by the Australian Research Council. Virgo is funded through the European Gravitational Observatory (EGO), by the French Centre National de Recherche Scientifique (CNRS), the Italian Istituto Nazionale di Fisica Nucleare (INFN) and the Dutch Nikhef, with contributions by institutions from Belgium, Germany, Greece, Hungary, Ireland, Japan, Monaco, Poland, Portugal, Spain. KAGRA is supported

by Ministry of Education, Culture, Sports, Science and Technology (MEXT), Japan Society for the Promotion of Science (JSPS) in Japan; National Research Foundation (NRF) and Ministry of Science and ICT (MSIT) in Korea; Academia Sinica (AS) and National Science and Technology Council (NSTC) in Taiwan. This document has been assigned the LIGO document number LIGO-P2400163.

APPENDIX

A. WAVEFORM SYSTEMATICS

LVK (2024) demonstrated that while not dominant with respect to statistical uncertainties, systematic errors due to the choice of the employed gravitational-wave models are not negligible. Moreover, GW230529 inhabits a parameter space previously unexplored through observations. In this appendix, we elucidate that systematic uncertainties hold minimal significance within the framework of population-informed priors. Furthermore, we assert that the findings presented in this study remain robust regardless of the specific model chosen.

To substantiate this claim, we perform the following analyses: (i) we measure the mismatch between the two waveform models, namely the *IMRPhenomNSBH* and *TEOBResumS-GIOTTO* (Akçay et al. 2019; Nagar et al. 2020a,b; Gonzalez et al. 2023), the latter being an Effective-One-Body model for compact objects informed by numerical relativity simulations of merging binary black holes and BHNS systems containing higher modes and tidal disruption (Buonanno & Damour 1999). This study uses posterior samples obtained when assuming the fiducial model. (ii) We assess the robustness of mass parameter measurements against modelling systematics when employing the aforementioned waveform models.

A.1. Comparison between *TEOBResumS-GIOTTO* and *IMRPhenomNSBH*

We quantify the discrepancy between the waveform models in terms of the match (or faithfulness) (Cutler & Flanagan 1994; Apostolatos 1995):

$$\mathcal{F} = \max_{t_{\text{ref}}, \phi_{\text{ref}}} \frac{(h|k)}{\sqrt{(h|h)(k|k)}}, \quad (\text{A1})$$

where t_{ref} and ϕ_{ref} are a reference time and phase, h and k are the two waveforms considered and

$$(h|k) = 4\Re \int_{f_{\text{min}}}^{f_{\text{max}}} \frac{\tilde{h}(f)\tilde{k}^*(f)}{S_n(f)} df. \quad (\text{A2})$$

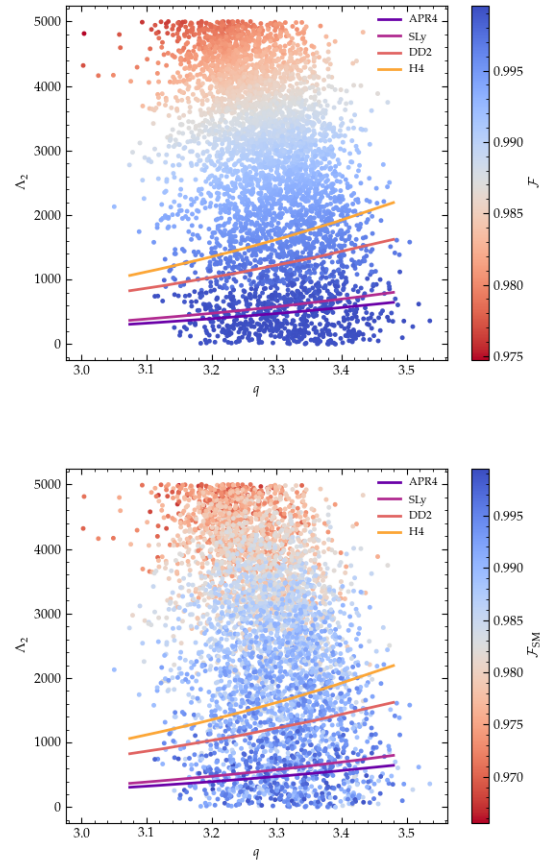


Figure 8. Match \mathcal{F} and sky-maximized match \mathcal{F}_{SM} between polarizations constructed using the dominant quadrupolar (top) and subdominant (bottom) modes of *TEOBResumS-GIOTTO* and *IMRPhenomNSBH*. We consider posterior samples from the fiducial PE and compute \mathcal{F} between 20 and 1796 Hz. Depending on whether higher modes are employed or not, we find median mismatches of about $\sim 1.4\%$ (0.8%) and maximum mismatches of $\sim 3\%$ ($\sim 2\%$), corresponding to systems with large tidal parameters $\Lambda_2 > 3000$. Overlaid, we also plot the tidal parameters obtained with a few selected EoSs assuming a fixed BH source frame mass of $4.2M_{\odot}$.

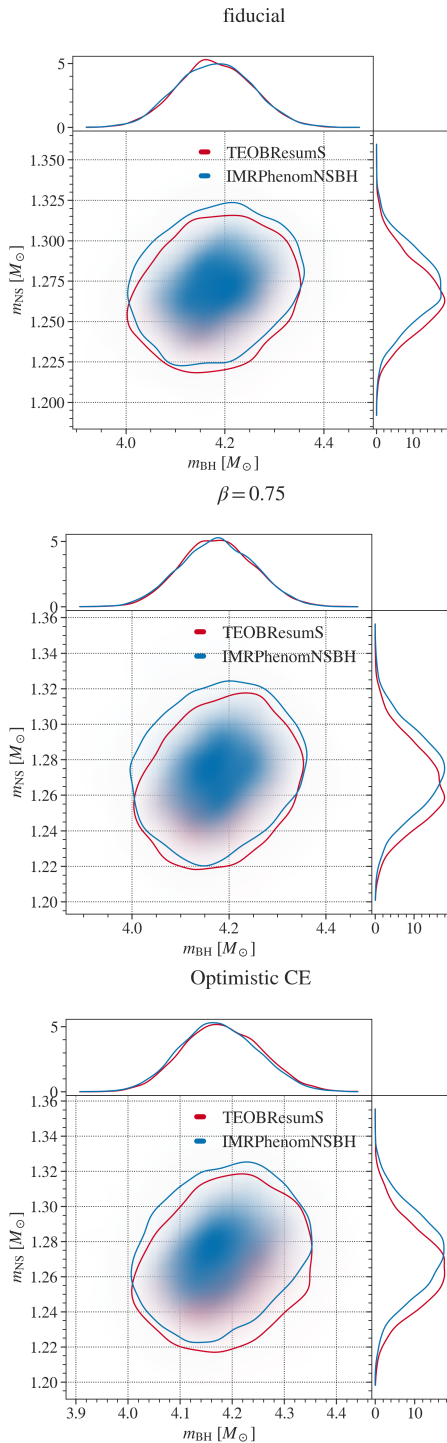


Figure 9. The posterior distribution of the primary and secondary source masses for two different waveform models — TEOBResumS-GIOTTO and IMRPhenomNSBH. Each contour shows the 90% credible intervals. We find that the resulting parameter estimates are robust to possible waveform systematics, with good agreement between the two waveform models.

Since TEOBResumS-GIOTTO contains higher-order radiation multipoles¹, the definition above is not independent of the extrinsic parameters of the binary. We, therefore, maximise over the sky position and polarization by computing the sky-maximized match \mathcal{F}_{SM} as defined in Harry et al. (2018); Chandra et al. (2022). This statistic reduces to the Eq. (A1) when only $(2, |2|)$ modes are employed. We then compute this quantity over the frequency interval $[20, 1796]$ Hz and employ the power spectral density S_n of GW230529. Crucially, to avoid noise artefacts in the fast Fourier transform, we generate the waveforms from 18 Hz and taper them at the beginning.

We find that the mismatches always lie below the 2.5% threshold when only $(2, |2|)$ modes are considered and below 3.5% when subdominant multipoles are included in the polarizations computation (see Fig. 8). As expected, both \mathcal{F} and \mathcal{F}_{SM} decrease with increasing tidal parameters: if one reduces the interval of Λ_2 considered to $[0, 3000]$, the maximum values for the figures above shift to 1.2% and 2.3% respectively. This is because neutron stars characterized by large values of Λ_2 are more easily disrupted, leading to growing differences in the model’s predictions in a region poorly explored by numerical relativity simulations.

To understand whether the matches obtained are “acceptable”, they should, in principle, be compared to some accuracy requirement, i.e. to some theoretical threshold below which one may expect waveform systematics to appear (Cutler & Flanagan 1994; Lindblom et al. 2008; Damour et al. 2011; Chatziioannou et al. 2017; Toubiana & Gair 2024). While correctly assessing accuracy requirements is largely a back-of-the-envelope estimate can be obtained employing the following threshold $\mathcal{F}_{\text{thrs}}$ (Damour et al. 2011; Chatziioannou et al. 2017):

$$\mathcal{F}_{\text{thrs}} = 1 - \frac{\epsilon}{2\rho^2}, \quad (\text{A3})$$

where ϵ is the number of intrinsic parameters of the system. This choice leads to $\mathcal{F}_{\text{thrs}} = 0.988$ ($\epsilon = 3$), smaller than $\sim 65\%$ of the matches computed when only $(2, |2|)$ modes are considered. When subdominant modes are further included in the analysis, inclination should be treated as an intrinsic source parameter and $\mathcal{F}_{\text{thrs}} = 0.984$, smaller than 58% of the mismatches computed. As such, though some differences between models are certainly present, one should not expect large biases to appear.

¹ In detail, we employ the $(\ell, |m|) = (2, 1), (2, 2), (3, 3), (4, 4)$ modes.

A.2. Re-analysis with *TEOBResumS*

We repeated some of the population-informed parameter estimations using the time-domain waveform model *TEOBResumS-GIOTTO*, as shown in Fig 9. The results indicate that the GW23059’s source mass parameters are robust against modelling systematics. This is consistent with the faithfulness study performed in the previous section. Although the models employ entirely independent descriptions of both point-mass and tidal sectors, differences are largely irrelevant: the high-frequency component of the data is dominated by noise and, as such, does not affect the inference. Additionally, our prior constrains the spins of the system components to be effectively zero, further minimizing differences between models.

B. KILONOVA LIGHTCURVES

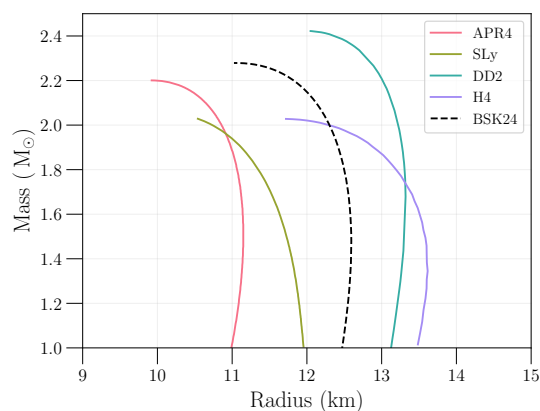


Figure 10. The mass-radius curves for the EoS chosen in this study. We also show the BSK24 EoS which was used by LVK (2024).

As noted in Sec. 4.3, the KNe light curves were generated using numerical recipes in Gupta et al. (2023). We only consider samples where the mass ratio is less than 4. We assume the electron fraction for the dynamical ejecta to be 0.1 and for the unbound disk ejecta to be 0.3 (Ekanger et al. 2023). The opacity values are obtained by fitting to data from Tanaka et al. (2020).

The four chosen EoSs in Sec. 4.3 span a wide range in the mass-radius diagram (see Fig. 10). This allows us to gauge the effect of different nuclear matter compositions on the expected electromagnetic counterpart. Notably, the BSK24 EoS (Goriely et al. 2013) – used by LVK (2024) – is contained within this range. Fig. 11 shows the results corresponding to the DD2 EoSs, which show similar features to those from H4.

To compare our results with Zhu et al. (2024), we, in Fig. 12, show the distribution of the peak luminosity in the *g* and *r* bands for the “fiducial” model and the DD2 EoS. While the two works get similar estimates for peak luminosities, our model results in dimmer KNe compared to the one used by Zhu et al. (2024). Furthermore, the maximum likelihood binary parameters correspond to a significantly fainter KNe, affecting the KNe’s detectability from such systems.

REFERENCES

2024. <https://arxiv.org/abs/2404.04248>
- Aasi, J., et al. 2015, *Class. Quant. Grav.*, 32, 074001, doi: [10.1088/0264-9381/32/7/074001](https://doi.org/10.1088/0264-9381/32/7/074001)
- Abbott, B. P., et al. 2017, *Phys. Rev. Lett.*, 119, 161101, doi: [10.1103/PhysRevLett.119.161101](https://doi.org/10.1103/PhysRevLett.119.161101)
- . 2019a, *Phys. Rev. X*, 9, 031040, doi: [10.1103/PhysRevX.9.031040](https://doi.org/10.1103/PhysRevX.9.031040)
- . 2019b, *Phys. Rev. X*, 9, 011001, doi: [10.1103/PhysRevX.9.011001](https://doi.org/10.1103/PhysRevX.9.011001)
- Abbott, R., et al. 2021, *Phys. Rev. X*, 11, 021053, doi: [10.1103/PhysRevX.11.021053](https://doi.org/10.1103/PhysRevX.11.021053)
- Akçay, S., Bernuzzi, S., Messina, F., et al. 2019, *Phys. Rev. D*, 99, 044051, doi: [10.1103/PhysRevD.99.044051](https://doi.org/10.1103/PhysRevD.99.044051)
- Akmal, A., Pandharipande, V. R., & Ravenhall, D. G. 1998, *Phys. Rev. C*, 58, 1804, doi: [10.1103/PhysRevC.58.1804](https://doi.org/10.1103/PhysRevC.58.1804)
- Alsing, J., Silva, H. O., & Berti, E. 2018, *Mon. Not. Roy. Astron. Soc.*, 478, 1377, doi: [10.1093/mnras/sty1065](https://doi.org/10.1093/mnras/sty1065)
- Antoniadis, J., Tauris, T. M., Ozel, F., et al. 2016. <https://arxiv.org/abs/1605.01665>
- Apostolatos, T. A. 1995, *Phys. Rev. D*, 52, 605, doi: [10.1103/PhysRevD.52.605](https://doi.org/10.1103/PhysRevD.52.605)
- Arnett, D. 1982, *The Astrophysical Journal*
- Arnett, W. D. 1980, *The Astrophysical Journal*, 237, 541, doi: [10.1086/157898](https://doi.org/10.1086/157898)
- Ashton, G., & Dietrich, T. 2022, *Nature Astron.*, 6, 961, doi: [10.1038/s41550-022-01707-x](https://doi.org/10.1038/s41550-022-01707-x)

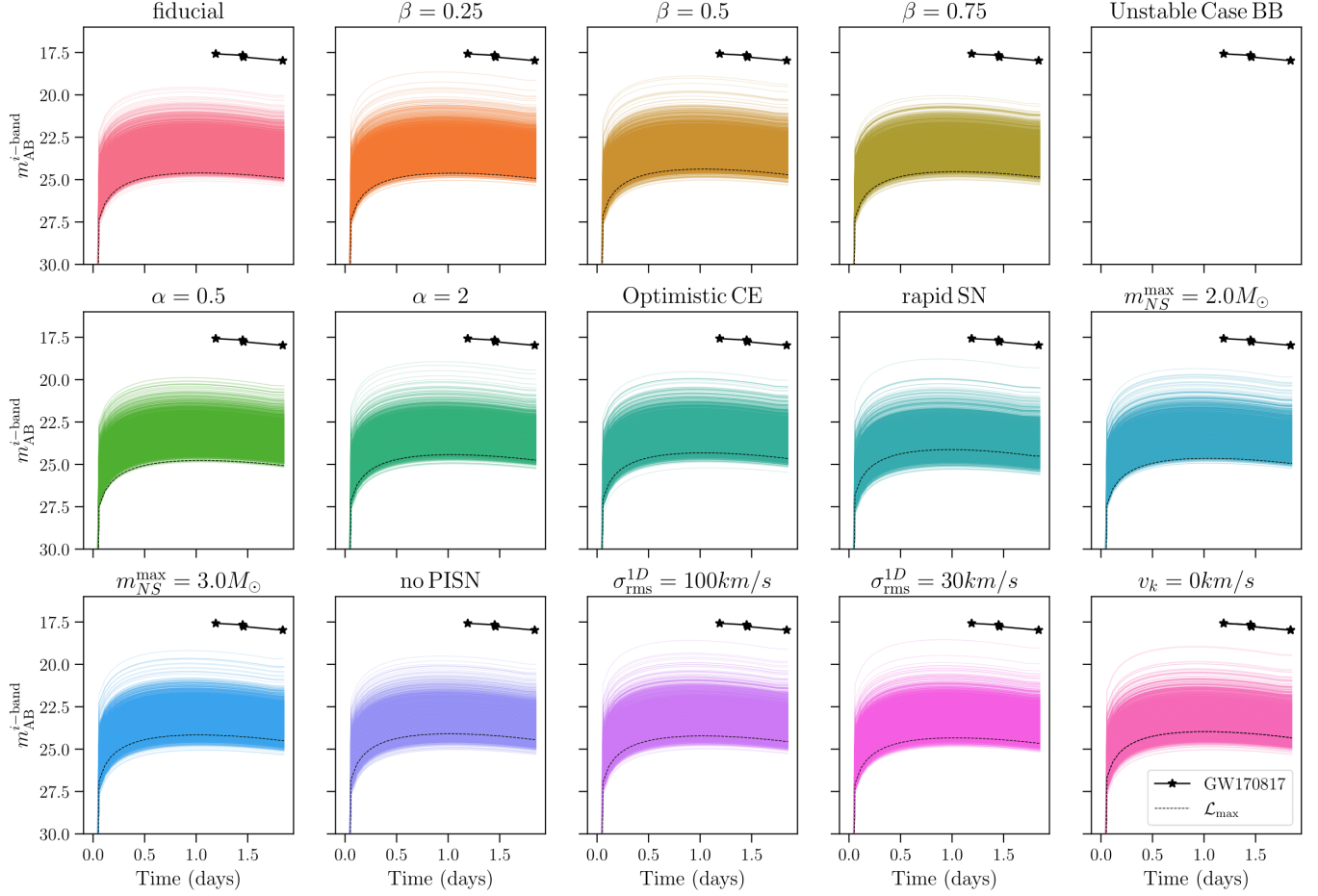


Figure 11. KNe light curves in the i -band corresponding to the different population models for the DD2 EoS. The dotted line shows the light curve associated with the maximum likelihood parameter estimates for each model.

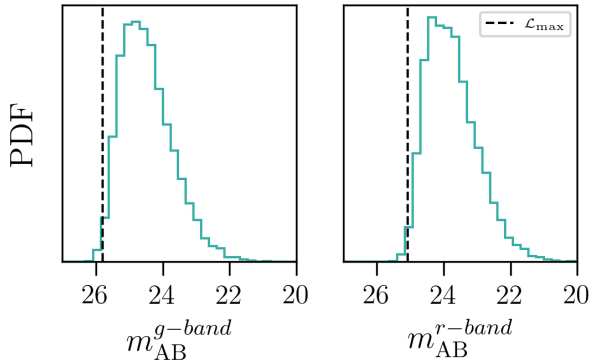


Figure 12. The distribution of the peak luminosity in the g and r bands for the DD2 EoS corresponding to samples from the “fiducial” population model. The black dotted line shows the peak luminosity corresponding to the maximum likelihood binary parameters.

Ashton, G., et al. 2019, *Astrophys. J. Suppl.*, 241, 27,

doi: [10.3847/1538-4365/ab06fc](https://doi.org/10.3847/1538-4365/ab06fc)

- Bailyn, C. D., Jain, R. K., Coppi, P., & Orosz, J. A. 1998, *Astrophys. J.*, 499, 367, doi: [10.1086/305614](https://doi.org/10.1086/305614)
- Barbieri, C., Salafia, O. S., Colpi, M., et al. 2019, *The Astrophysical Journal Letters*, 887, L35, doi: [10.3847/2041-8213/ab5c1e](https://doi.org/10.3847/2041-8213/ab5c1e)
- Barbieri, C., Salafia, O. S., Perego, A., Colpi, M., & Ghirlanda, G. 2020, *Eur. Phys. J. A*, 56, 8, doi: [10.1140/epja/s10050-019-00013-x](https://doi.org/10.1140/epja/s10050-019-00013-x)
- Belczynski, K., Bulik, T., Fryer, C. L., et al. 2010, *ApJ*, 714, 1217, doi: [10.1088/0004-637X/714/2/1217](https://doi.org/10.1088/0004-637X/714/2/1217)
- Belczynski, K., Romagnolo, A., Olejak, A., et al. 2022, *ApJ*, 925, 69, doi: [10.3847/1538-4357/ac375a](https://doi.org/10.3847/1538-4357/ac375a)
- Branchesi, M., et al. 2023, *JCAP*, 07, 068, doi: [10.1088/1475-7516/2023/07/068](https://doi.org/10.1088/1475-7516/2023/07/068)
- Breschi, M., Gamba, R., Carullo, G., et al. 2024. <https://arxiv.org/abs/2401.03750>
- Broekgaarden, F. S., & Berger, E. 2021, *ApJL*, 920, L13, doi: [10.3847/2041-8213/ac2832](https://doi.org/10.3847/2041-8213/ac2832)

- Broekgaarden, F. S., Berger, E., Neijssel, C. J., et al. 2021, *Mon. Not. Roy. Astron. Soc.*, 508, 5028, doi: [10.1093/mnras/stab2716](https://doi.org/10.1093/mnras/stab2716)
- Buonanno, A., & Damour, T. 1999, *Phys. Rev. D*, 59, 084006, doi: [10.1103/PhysRevD.59.084006](https://doi.org/10.1103/PhysRevD.59.084006)
- Chabanat, E., Bonche, P., Haensel, P., Meyer, J., & Schaeffer, R. 1998, *Nucl. Phys. A*, 635, 231, doi: [10.1016/S0375-9474\(98\)00180-8](https://doi.org/10.1016/S0375-9474(98)00180-8)
- Chandra, K., Calderón Bustillo, J., Pai, A., & Harry, I. W. 2022, *Phys. Rev. D*, 106, 123003, doi: [10.1103/PhysRevD.106.123003](https://doi.org/10.1103/PhysRevD.106.123003)
- Chattopadhyay, D., Stevenson, S., Broekgaarden, F., Antonini, F., & Belczynski, K. 2022, *MNRAS*, 513, 5780, doi: [10.1093/mnras/stac1283](https://doi.org/10.1093/mnras/stac1283)
- Chattopadhyay, D., Stevenson, S., Hurley, J. R., Bailes, M., & Broekgaarden, F. 2021, *Mon. Not. Roy. Astron. Soc.*, 504, 3682, doi: [10.1093/mnras/stab973](https://doi.org/10.1093/mnras/stab973)
- Chatziioannou, K., Klein, A., Yunes, N., & Cornish, N. 2017, *Phys. Rev. D*, 95, 104004, doi: [10.1103/PhysRevD.95.104004](https://doi.org/10.1103/PhysRevD.95.104004)
- Chatzopoulos, E., Craig Wheeler, J., & Vinko, J. 2012, doi: [10.1088/0004-637X/746/2/121](https://doi.org/10.1088/0004-637X/746/2/121)
- Cornish, N. J. 2010. <https://arxiv.org/abs/1007.4820>
- . 2021, *Phys. Rev. D*, 104, 104054, doi: [10.1103/PhysRevD.104.104054](https://doi.org/10.1103/PhysRevD.104.104054)
- Cutler, C., & Flanagan, E. E. 1994, *Phys. Rev. D*, 49, 2658, doi: [10.1103/PhysRevD.49.2658](https://doi.org/10.1103/PhysRevD.49.2658)
- Damour, T., Nagar, A., & Trias, M. 2011, *Phys. Rev. D*, 83, 024006, doi: [10.1103/PhysRevD.83.024006](https://doi.org/10.1103/PhysRevD.83.024006)
- Dietrich, T., Samajdar, A., Khan, S., et al. 2019, *Phys. Rev. D*, 100, 044003, doi: [10.1103/PhysRevD.100.044003](https://doi.org/10.1103/PhysRevD.100.044003)
- Douchin, F., & Haensel, P. 2001, *Astron. Astrophys.*, 380, 151, doi: [10.1051/0004-6361:20011402](https://doi.org/10.1051/0004-6361:20011402)
- Ekanger, N., Bhattacharya, M., & Horiuchi, S. 2023, *Mon. Not. Roy. Astron. Soc.*, 525, 2040, doi: [10.1093/mnras/stad2348](https://doi.org/10.1093/mnras/stad2348)
- Farah, A. M., Fishbach, M., Essick, R., Holz, D. E., & Galaudage, S. 2022, *Astrophys. J.*, 931, 108, doi: [10.3847/1538-4357/ac5f03](https://doi.org/10.3847/1538-4357/ac5f03)
- Farr, W. M., & Chatziioannou, K. 2020, *Research Notes of the AAS*, 4, 65, doi: [10.3847/2515-5172/ab9088](https://doi.org/10.3847/2515-5172/ab9088)
- Farr, W. M., Sravan, N., Cantrell, A., et al. 2011, *Astrophys. J.*, 741, 103, doi: [10.1088/0004-637X/741/2/103](https://doi.org/10.1088/0004-637X/741/2/103)
- Fishbach, M., Essick, R., & Holz, D. E. 2020, *Astrophys. J. Lett.*, 899, L8, doi: [10.3847/2041-8213/aba7b6](https://doi.org/10.3847/2041-8213/aba7b6)
- Fonseca, E., et al. 2021, *Astrophys. J. Lett.*, 915, L12, doi: [10.3847/2041-8213/ac03b8](https://doi.org/10.3847/2041-8213/ac03b8)
- Foucart, F., Buchman, L., Duez, M. D., et al. 2013, *Phys. Rev. D*, 88, 064017, doi: [10.1103/PhysRevD.88.064017](https://doi.org/10.1103/PhysRevD.88.064017)
- Foucart, F., Deaton, M. B., Duez, M. D., et al. 2014, *Phys. Rev. D*, 90, 024026, doi: [10.1103/PhysRevD.90.024026](https://doi.org/10.1103/PhysRevD.90.024026)
- Fragos, T., & McClintock, J. E. 2015, *Astrophys. J.*, 800, 17, doi: [10.1088/0004-637X/800/1/17](https://doi.org/10.1088/0004-637X/800/1/17)
- Fryer, C. L., Belczynski, K., Wiktorowicz, G., et al. 2012, *ApJ*, 749, 91, doi: [10.1088/0004-637X/749/1/91](https://doi.org/10.1088/0004-637X/749/1/91)
- Garcia, A. M., Torrey, P., Ellison, S., et al. 2024, arXiv e-prints, arXiv:2403.08856, doi: [10.48550/arXiv.2403.08856](https://doi.org/10.48550/arXiv.2403.08856)
- Glendenning, N. K., & Moszkowski, S. A. 1991, *Phys. Rev. Lett.*, 67, 2414, doi: [10.1103/PhysRevLett.67.2414](https://doi.org/10.1103/PhysRevLett.67.2414)
- Godzieba, D. A., Radice, D., & Bernuzzi, S. 2021, *Astrophys. J.*, 908, 122, doi: [10.3847/1538-4357/abd4dd](https://doi.org/10.3847/1538-4357/abd4dd)
- Gonzalez, A., Gamba, R., Breschi, M., et al. 2023, *Phys. Rev. D*, 107, 084026, doi: [10.1103/PhysRevD.107.084026](https://doi.org/10.1103/PhysRevD.107.084026)
- Goriely, S., Chamel, N., & Pearson, J. M. 2013, *Phys. Rev. C*, 88, 061302, doi: [10.1103/PhysRevC.88.061302](https://doi.org/10.1103/PhysRevC.88.061302)
- Guillochon, J., Parrent, J., Kelley, L. Z., & Margutti, R. 2017, *The Astrophysical Journal*, 835, 64, doi: [10.3847/1538-4357/835/1/64](https://doi.org/10.3847/1538-4357/835/1/64)
- Gupta, I. 2023, *Mon. Not. Roy. Astron. Soc.*, 524, 3537, doi: [10.1093/mnras/stad2115](https://doi.org/10.1093/mnras/stad2115)
- . 2024. <https://arxiv.org/abs/2402.07075>
- Gupta, I., Borhanian, S., Dhani, A., et al. 2023, *Phys. Rev. D*, 107, 124007, doi: [10.1103/PhysRevD.107.124007](https://doi.org/10.1103/PhysRevD.107.124007)
- Gupta, I., Kashyap, R., & Bhattacharya, M. 2024
- Harry, I., Calderón Bustillo, J., & Nitz, A. 2018, *Phys. Rev. D*, 97, 023004, doi: [10.1103/PhysRevD.97.023004](https://doi.org/10.1103/PhysRevD.97.023004)
- Hempel, M., & Schaffner-Bielich, J. 2010, *Nucl. Phys. A*, 837, 210, doi: [10.1016/j.nuclphysa.2010.02.010](https://doi.org/10.1016/j.nuclphysa.2010.02.010)
- Hurley, J. R., Pols, O. R., & Tout, C. A. 2000, *MNRAS*, 315, 543, doi: [10.1046/j.1365-8711.2000.03426.x](https://doi.org/10.1046/j.1365-8711.2000.03426.x)
- Ivanova, N., Justham, S., Chen, X., et al. 2013, *A&A Rv*, 21, 59, doi: [10.1007/s00159-013-0059-2](https://doi.org/10.1007/s00159-013-0059-2)
- Ivezić, v., et al. 2019, *Astrophys. J.*, 873, 111, doi: [10.3847/1538-4357/ab042c](https://doi.org/10.3847/1538-4357/ab042c)
- Kashyap, R., Raman, G., & Ajith, P. 2019, *Astrophys. J. Lett.*, 886, L19, doi: [10.3847/2041-8213/ab543f](https://doi.org/10.3847/2041-8213/ab543f)
- Kawaguchi, K., Domoto, N., Fujibayashi, S., et al. 2024. <https://arxiv.org/abs/2404.15027>
- Khan, S., Husa, S., Hannam, M., et al. 2016, *Phys. Rev. D*, 93, 044007, doi: [10.1103/PhysRevD.93.044007](https://doi.org/10.1103/PhysRevD.93.044007)
- Krishna, K., Vijaykumar, A., Ganguly, A., et al. 2023. <https://arxiv.org/abs/2312.06009>
- Krüger, C. J., & Foucart, F. 2020. <https://arxiv.org/abs/2002.07728>
- Krüger, C. J., & Foucart, F. 2020, *Phys. Rev. D*, 101, 103002, doi: [10.1103/PhysRevD.101.103002](https://doi.org/10.1103/PhysRevD.101.103002)

- Kyutoku, K., Kiuchi, K., Sekiguchi, Y., Shibata, M., & Taniguchi, K. 2018, *Physical Review D*, 97, 023009, doi: [10.1103/PhysRevD.97.023009](https://doi.org/10.1103/PhysRevD.97.023009)
- Kyutoku, K., Shibata, M., & Taniguchi, K. 2021, *Living Reviews in Relativity*, 24, 5, doi: [10.1007/s41114-021-00033-4](https://doi.org/10.1007/s41114-021-00033-4)
- Lackey, B. D., Nayyar, M., & Owen, B. J. 2006, *Phys. Rev. D*, 73, 024021, doi: [10.1103/PhysRevD.73.024021](https://doi.org/10.1103/PhysRevD.73.024021)
- Langeroodi, D., Hjorth, J., Chen, W., et al. 2023, *ApJ*, 957, 39, doi: [10.3847/1538-4357/acdbcl](https://doi.org/10.3847/1538-4357/acdbcl)
- Lattimer, J. M., & Schramm, D. N. 1974, *The Astrophysical journal*, 192, L145, doi: [10.1086/181612](https://doi.org/10.1086/181612)
- . 1976, *The Astrophysical journal*, 210, 549, doi: [10.1086/154860](https://doi.org/10.1086/154860)
- Lindblom, L., Owen, B. J., & Brown, D. A. 2008, *Phys. Rev. D*, 78, 124020, doi: [10.1103/PhysRevD.78.124020](https://doi.org/10.1103/PhysRevD.78.124020)
- Littenberg, T. B., & Cornish, N. J. 2015, *Phys. Rev. D*, 91, 084034, doi: [10.1103/PhysRevD.91.084034](https://doi.org/10.1103/PhysRevD.91.084034)
- Ma, L., & Fuller, J. 2019, *Mon. Not. Roy. Astron. Soc.*, 488, 4338, doi: [10.1093/mnras/stz2009](https://doi.org/10.1093/mnras/stz2009)
- Mandel, I., & Broekgaarden, F. S. 2022, *Living Rev. Rel.*, 25, 1, doi: [10.1007/s41114-021-00034-3](https://doi.org/10.1007/s41114-021-00034-3)
- Mandel, I., & Fragos, T. 2020, *Astrophys. J. Lett.*, 895, L28, doi: [10.3847/2041-8213/ab8e41](https://doi.org/10.3847/2041-8213/ab8e41)
- Metzger, B. D. 2017, *Living Rev. Rel.*, 20, 3, doi: [10.1007/s41114-017-0006-z](https://doi.org/10.1007/s41114-017-0006-z)
- Miller, M. C., et al. 2021, *Astrophys. J. Lett.*, 918, L28, doi: [10.3847/2041-8213/ac089b](https://doi.org/10.3847/2041-8213/ac089b)
- Nagar, A., Pratten, G., Riemenschneider, G., & Gamba, R. 2020a, *Phys. Rev. D*, 101, 024041, doi: [10.1103/PhysRevD.101.024041](https://doi.org/10.1103/PhysRevD.101.024041)
- Nagar, A., Riemenschneider, G., Pratten, G., Rettegno, P., & Messina, F. 2020b, *Phys. Rev. D*, 102, 024077, doi: [10.1103/PhysRevD.102.024077](https://doi.org/10.1103/PhysRevD.102.024077)
- Ozel, F., Psaltis, D., Narayan, R., & McClintock, J. E. 2010, *Astrophys. J.*, 725, 1918, doi: [10.1088/0004-637X/725/2/1918](https://doi.org/10.1088/0004-637X/725/2/1918)
- Raaijmakers, G., et al. 2021, *Astrophys. J.*, 922, 269, doi: [10.3847/1538-4357/ac222d](https://doi.org/10.3847/1538-4357/ac222d)
- Ray, A., Magaña Hernandez, I., Mohite, S., Creighton, J., & Kapadia, S. 2023, *Astrophys. J.*, 957, 37, doi: [10.3847/1538-4357/acf452](https://doi.org/10.3847/1538-4357/acf452)
- Read, J. S., Lackey, B. D., Owen, B. J., & Friedman, J. L. 2009, *Phys. Rev. D*, 79, 124032, doi: [10.1103/PhysRevD.79.124032](https://doi.org/10.1103/PhysRevD.79.124032)
- Romani, R. W., Kandel, D., Filippenko, A. V., Brink, T. G., & Zheng, W. 2022, *Astrophys. J. Lett.*, 934, L17, doi: [10.3847/2041-8213/ac8007](https://doi.org/10.3847/2041-8213/ac8007)
- Speagle, J. S. 2020, *Mon. Not. Roy. Astron. Soc.*, 493, 3132, doi: [10.1093/mnras/staa278](https://doi.org/10.1093/mnras/staa278)
- Tanaka, M., Kato, D., Gaigalas, G., & Kawaguchi, K. 2020, *Mon. Not. Roy. Astron. Soc.*, 496, 1369, doi: [10.1093/mnras/staa1576](https://doi.org/10.1093/mnras/staa1576)
- Thompson, J. E., Fauchon-Jones, E., Khan, S., et al. 2020, *Phys. Rev. D*, 101, 124059, doi: [10.1103/PhysRevD.101.124059](https://doi.org/10.1103/PhysRevD.101.124059)
- Toubiana, A., & Gair, J. R. 2024. <https://arxiv.org/abs/2401.06845>
- Typel, S., Ropke, G., Klahn, T., Blaschke, D., & Wolter, H. H. 2010, *Phys. Rev. C*, 81, 015803, doi: [10.1103/PhysRevC.81.015803](https://doi.org/10.1103/PhysRevC.81.015803)
- Villar, V. A., et al. 2017, *Astrophys. J. Lett.*, 851, L21, doi: [10.3847/2041-8213/aa9c84](https://doi.org/10.3847/2041-8213/aa9c84)
- Vinciguerra, S., et al. 2024, *Astrophys. J.*, 961, 62, doi: [10.3847/1538-4357/acfb83](https://doi.org/10.3847/1538-4357/acfb83)
- Zackay, B., Dai, L., & Venumadhav, T. 2018. <https://arxiv.org/abs/1806.08792>
- Zappa, F., Bernuzzi, S., Pannarale, F., Mapelli, M., & Giacobbo, N. 2019, *Phys. Rev. Lett.*, 123, 041102, doi: [10.1103/PhysRevLett.123.041102](https://doi.org/10.1103/PhysRevLett.123.041102)
- Zhu, J.-P., Hu, R.-C., Kang, Y., et al. 2024. <https://arxiv.org/abs/2404.10596>